Oil Shale, 2024, Vol. 41, No. 1, pp. 26–48
doi: https://doi.org/10.3176/oil.2024.1.02
ISSN 0208-189X

Groundwater environmental impact caused by in-situ pyrolysis of oil shale

Ling Yang[a,b], Jian Liu[b,c,d]*, Haoran Yi[e], Xiaogang Zhang[b,c], Yaozong Wang[b,c,f], Shenjun Qin[b,c]

[a] School of Water Conservancy and Hydroelectric Power, Hebei University of Engineering, Handan, Hebei 056038, China
[b] School of Geosciences and Engineering, Hebei University of Engineering, Handan, Hebei 056038, China
[c] Collaborative Innovation Center of the Comprehensive Development and Utilization of Coal Resources, Handan, Hebei 056038, China
[d] Key Lab of In-situ Property-improving Mining of Ministry of Education, Taiyuan University of Technology, Taiyuan, Shanxi 030024, China
[e] Hydrogeology Bureau, China National Administration of Coal Geology, Handan, Hebei 056004, China
[f] Geological Exploration Technology Center, Bureau of Geology and Mineral Exploration and Development of Hebei Province, Shijiazhuang, Hebei 050081, China

Received 24 October 2023, accepted 19 January 2024, available online 16 February 2024

Abstract. *Based on a sample of oil shale from the Lucaogou Formation in Shichanggou, Xinjiang, China, the mechanism of changes in the physical and mechanical properties of oil shale during in-situ pyrolysis was systematically analyzed, and combined with the kinetics of the pyrolysis reaction, a constitutive model of permeability change during the in-situ pyrolysis of oil shale was established. By leaching experiments, the changes in the physicochemical parameters and pollutant concentration of oil shale immersion solution under different pyrolysis temperatures were studied. Basing on the theoretical permeability value and pollutant concentration under in-situ pyrolysis conditions, a hydrogeological model was established to simulate groundwater pollution caused by the in-situ pyrolysis of oil shale. The results showed that the permeability of oil shale after in-situ pyrolysis increased by three orders of magnitude, changing from a water-proof layer before pyrolysis to a weakly permeable layer after pyrolysis. However, the permeability of oil shale after complete pyrolysis at 600 °C was only 2.062 mD and still very low, and the pollutants had low concentration and were mainly concentrated in the pyrolyzed oil shale layer. The in-situ pyrolysis of oil shale would not pollute the groundwater in the mining area, but the pH of groundwater would gradually increase with rising pyrolysis temperatures. At 600 °C, pH even increased to*

* Corresponding author, 5102135@163.com

11.68, which is strongly alkaline. It is suggested that the pyrolysis temperature should be 400–500 °C.

Keywords: *oil shale, in-situ pyrolysis, permeability constitutive model, groundwater pollution.*

1. Introduction

In-situ pyrolysis is a new method for mining oil shale that can generate shale oil and combustible gas products by injecting heat into underground oil shale formations. Compared with the traditional well mining method, the emerging in-situ pyrolysis mining technology has the advantages of less processing, lower costs, higher efficiency and less land occupation, which makes it an important method of oil shale exploration in the future. However, with the precipitation of pyrolysis products, after in-situ pyrolysis oil shale becomes loose and porous, and the permeability increases significantly, causing oil shale to change from the original aquiclude to a permeable layer, which changes the hydrogeological environment of the mining area and even induces groundwater pollution. Before large-scale industrial application of the in-situ pyrolysis process for oil shale, it is urgent to carry out research on groundwater pollution in the in-situ pyrolysis mining area, analyze hydrogeological environmental changes and pollutant transport laws, and put forward suggestions for process optimization, which is undoubtedly of great significance.

In recent years, domestic and foreign scholars have carried out relevant preliminary research on the changes in the permeability and environmental effects of oil shale induced by the in-situ pyrolysis process. In terms of permeability characteristics, earlier research mainly focused on the correspondence between the pore characteristics pyrolysis and the permeability of oil shale. Porosity is the controlling factor in permeability changes, and temperature can significantly affect the evolution of the pore structure of oil shale [1, 2]. The porosity and permeability of oil shale in the original state are both low. With the increase of pyrolysis temperature and the precipitation of oil and gas substances, the pore diameter gradually increases, pore roughness and surface irregularity gradually increase, new pores are continuously formed and gradually connected, permeability channels are formed, and porosity and permeability increase synchronously and rapidly [3–5].

With the continuous deepening of basic research, researchers have gradually realized that the coupling effect of temperature and pressure has an important impact on porosity and permeability [6–8]. Under the influence of temperature and pressure, the pore and fissure structure of oil shale undergo fundamental and irreversible changes, causing oil shale to change from a dense and low-porosity state at room temperature to a state of extremely developed pores after pyrolysis at high temperature and high pressure, while

permeability also presents synchronous changes [9–11]. However, these research results basically focus on the comparative study of changes in the porosity and permeability of oil shale before and after pyrolysis, and are mainly qualitative descriptions.

Since in-situ pyrolysis is an emerging process, there are currently few studies on the environmental impact of this technology, and the existing research is focused on the impact on the atmosphere and ecological environment [12–14]. However, there are few reports on the environmental impact on groundwater that is most likely to be caused by in-situ pyrolysis mining of oil shale. This is mainly due to the difficulty in achieving real-time continuous observations of relevant parameters during the in-situ pyrolysis of oil shale, which undoubtedly complicates the research on the environmental impact on groundwater in the in-situ pyrolysis mining area.

2. Experiments and research methods

In response to the aforementioned problems, this study analyzed the change mechanism of oil shale permeability, established an oil shale permeability model during in-situ pyrolysis, and carried out relevant physical and mechanical experiments to verify the model. Combined with the immersion experiment, the physical and chemical parameters and pollutant concentration of the soaking liquid were obtained. Groundwater pollution in the in-situ pyrolysis of oil shale was studied with the groundwater simulation software MODFLOW.

2.1. Experimental scheme

2.1.1. Thermogravimetric experiment

An appropriate amount of ground oil shale (diameter ≤ 0.2 mm) was placed in the thermogravimetric analyzer (Setsys Evolution 16/18), and the quality of the sample was measured. High purity argon was used as the carrier gas, and the heating rate (30 °C/min) and the final temperature (800 °C) were set. The heating furnace was started and the change in oil shale sample quality was measured with increasing temperature.

2.1.2. Physical and mechanical experiments

The cylindrical oil shale specimens ($\Phi 25 \times 50$ mm; three samples were allocated for each pyrolysis condition) were placed in the muffle furnace (STM-30-12), high purity nitrogen was injected, the heating rate was set at 30 °C/min, and the target temperatures were 350, 400, 450, 500 and 600 °C. After reaching each target temperature, the temperature remained constant for 30, 15, 30, 45 and 60 minutes, then heating stopped, and the specimens were cooled to room temperature naturally. A pulse permeability tester (Smartperm III)

and rock mechanics testing machine (RIST-415) were used to measure the permeability, compressive strength and elastic modulus of oil shale specimens under different pyrolysis conditions. Then, the residues of damaged specimens (diameter <5 mm) under each pyrolysis condition were selected, and the porosities were measured by the mercury porosimeter (PoreMaster 33).

2.1.3. Immersion experiment

The pollutants leaching from oil shale after pyrolysis are the main culprits causing groundwater contamination in in-situ pyrolysis mining areas. To evaluate the situation of groundwater pollution caused by oil shale residue after pyrolysis, this study conducted leaching experiments on oil shale after full pyrolysis under different working conditions. Firstly, the oil shale samples under various pyrolysis conditions were crushed. Then, according to a mass ratio of 1:10, 20 g of oil shale powder was immersed in 200 ml of ultrapure water for 15 days, and the pH and electrical conductivity of the leaching solution were measured by the multiparameter water quality detector (Hach HQ30d). The concentrations of common heavy metal pollutants (lead, cadmium and total chromium) and organic pollutants (polycyclic aromatic hydrocarbons) in groundwater were determined by atomic absorption spectrophotometry (TAS-990) and liquid chromatography (Shimadzu LC-2030).

2.2. Method for establishing the oil shale permeability model during in-situ pyrolysis

Kerogen is the main pyrolysis target of oil shale. With the precipitation of pyrolysis products, such as shale oil and pyrolysis gas, oil shale gradually becomes loose and porous, and the closely related porosity and permeability also change synchronously. Under in-situ conditions, affected by confining pressure, oil shale undergoes compression deformation, resulting in changes in porosity, which in turn affects permeability. The deformation characteristics of oil shale can be characterized by the elastic modulus. Therefore, to study the rule of change in oil shale permeability during in-situ pyrolysis, it is necessary to establish the quantitative relationship between the elastic modulus, porosity and permeability; i.e., to establish a quantitative model of oil shale permeability during in-situ pyrolysis.

Based on the nature of pyrolysis, this research intended to first establish an oil shale porosity model and elastic modulus model during pyrolysis, then combine in-situ confining pressure conditions with rock mechanics theory, organically combine the porosity model and elastic modulus model to establish a model of oil shale porosity change during in-situ pyrolysis, and then combine the quantitative relationship between permeability and porosity. Finally, the permeability model of oil shale during in-situ pyrolysis was built, and the law of permeability variation was studied.

2.2.1. Method for establishing the porosity model of oil shale during pyrolysis

The pyrolysis of kerogen is the main reason for the porosity change in oil shale. Assuming that the pyrolysis products of kerogen are generated and then escape immediately, the porosity of oil shale during pyrolysis can be expressed as follows:

$$n' = n_c + \Delta n = n_c + \frac{m \cdot \alpha / \rho_o - m_c \cdot \alpha / \rho_c}{M / \rho_s} \times 100\% = n_c + \frac{p_o \cdot \alpha \cdot \rho_s}{\rho_o} - \frac{p_c \cdot \alpha \cdot \rho_s}{\rho_c}, \quad (1)$$

where M is the mass of oil shale, m is the mass of kerogen, m_c is the mass of carbon residue, ρ_s is the density of oil shale, ρ_o is the density of kerogen, ρ_c is the density of carbon residue, p_o is the content of kerogen, p_c is the content of carbon residue in oil shale, n_c is the initial porosity of oil shale, n' is the porosity of oil shale during pyrolysis, Δn is the change in the porosity of oil shale during pyrolysis, and α is the pyrolysis conversion rate of kerogen.

2.2.2. Method for establishing the elastic modulus model of oil shale during pyrolysis

Under high-temperature conditions, kerogen melts from solid to liquid. Under external loads, the pore pressure in oil shale is mainly provided by molten liquid kerogen. The thermal decomposition and evacuation of kerogen results in a decrease in pore pressure and an increase in effective stress, which in turn leads to an increase in strain and a decrease in the elastic modulus of oil shale. In addition, the decrease in the compressive strength of the oil shale skeleton at elevated temperatures affects the elastic modulus. In summary, the thermal decomposition of kerogen and the thermal damage of the oil shale skeleton during high-temperature pyrolysis are the main reasons for the change in the elastic modulus of oil shale.

Assuming that the pyrolysis products of kerogen are generated and then escape immediately, under the condition of equal strain, the elastic modulus model of oil shale during pyrolysis can be established as follows:

$$\frac{\sigma}{E} = \frac{\sigma_t}{E_t} = \frac{\sigma - \Delta\sigma - \Delta u}{E_t} = \frac{\sigma' + u_t}{E_t}, \quad (2)$$

$$E_t = \frac{E \cdot (\sigma' + u_t)}{\sigma} = \frac{E \cdot [\sigma' + u(1-\alpha)]}{\sigma}, \quad (3)$$

where E and σ are the elastic modulus and compressive strength of oil shale before pyrolysis, respectively, u is the pore pressure, E_t and σ_t are the elastic modulus and compressive strength of oil shale at any time during pyrolysis, respectively, $\Delta\sigma$ is the attenuation part of the compressive strength of the oil shale skeleton, Δu is the pore pressure provided by the pyrolysis part of kerogen, σ' is the compressive strength of the oil shale skeleton, and u_t is the pore pressure of oil shale during pyrolysis.

2.2.3. Method for establishing the porosity model of oil shale during in-situ pyrolysis

Under in-situ confining pressure, the change in the elastic modulus of oil shale during pyrolysis inevitably leads to the compression deformation of oil shale, which leads to synchronous changes in porosity and permeability. To make the established model of the change in oil shale porosity during in-situ pyrolysis reflect the physical essence without causing the model to be overly complicated, the following basic assumptions are introduced in this study:

1. The compression deformation of oil shale is linear elastic deformation.
2. The compression deformation of oil shale shows the shrinkage of its internal pores.
3. During compression deformation, oil shale has no new fractures.
4. There is equal horizontal confining pressure, i.e., $\sigma_2 = \sigma_3 = \dfrac{\sigma_1 \cdot \mu}{1-\mu}$.

According to the above assumptions and in combination with classical rock mechanics theory [15], the following relationship is obtained:

$$\sigma_m = \frac{\sigma_1 + \sigma_2 + \sigma_3}{3} = \frac{\sigma_1(1+\mu)}{3(1-\mu)} , \tag{4}$$

$$E_k = \frac{E_t}{3(1-2\mu)} , \tag{5}$$

$$\varepsilon_k = \frac{\sigma_m}{E_k} = \frac{\sigma_1(1+\mu)(1-2\mu)}{(1-\mu)E_t} . \tag{6}$$

The quantitative model of the porosity change in oil shale under in-situ conditions is established as follows:

$$n'' = \frac{V_p - V_t \cdot \varepsilon_k}{V_t(1-\varepsilon_k)} = \frac{n' - \varepsilon_k}{1-\varepsilon_k} , \tag{7}$$

where n'' is the porosity of oil shale at any time during in-situ pyrolysis, $n' = \dfrac{V_p}{V_t}$ is the porosity of oil shale at the corresponding time during pyrolysis under no pressure, V_p is the pore volume of oil shale at the corresponding time during pyrolysis under no pressure, V_t is the volume of oil shale at the corresponding time during pyrolysis under no pressure, ε_k is the volume strain of oil shale at the corresponding time during pyrolysis, E_k is the bulk modulus of oil shale at the corresponding time during pyrolysis, μ is the Poisson's ratio of oil shale, and σ_1, σ_2 and σ_3 are the three principal stresses.

2.2.4. Establishment of the permeability model of oil shale during in-situ pyrolysis

The permeability and porosity of rock masses are closely related, but due to the complexity of the pore structure, the constitutive relationship between the two is extremely complex, and there is currently a lack of corresponding physical constitutive models. Previous studies have found that the relationship between the porosity and permeability of oil shale approximately follows the most famous semiempirical formula in the field of porous media seepage, the Kozeny–Carman equation [16]:

$$k = k_0 (\frac{n}{n_0})^3 , \tag{8}$$

where k is the permeability of oil shale and k_0 is the initial permeability of oil shale.

The quantitative calculation model of oil shale permeability during in-situ pyrolysis is obtained by substituting Equation (7) into Equation (8):

$$k = k_0 \left[\frac{n' \cdot E_t - P}{(E_t - P) n_0} \right]^3 . \tag{9}$$

2.3. Methods for researching groundwater pollution in the in-situ pyrolysis mining area of oil shale

Based on the geological data of the study area, a hydrogeological physical model was constructed. Basic parameters were provided by the aforementioned physical and mechanical model of the in-situ pyrolysis of oil shale. With the immersion experimental results as the pollutant source concentration, groundwater pollution in the in-situ pyrolysis mining area under different pyrolysis temperature conditions (400, 500 and 600 °C) was simulated with the MODFLOW software.

3. Results

3.1. Basic properties of oil shale

The oil shale used in this study was taken from the Lucaogou Formation in Shichanggou, Xinjiang, and the basic industrial parameters are shown in Table 1.

Table 1. Basic industrial parameters of Xinjiang oil shale

Moisture, %	Ash, %	Volatiles, %	Fixed carbon, %	Oil content, %	Calorific value, MJ/kg
4.31	53.27	35.18	7.11	11.08	6.88

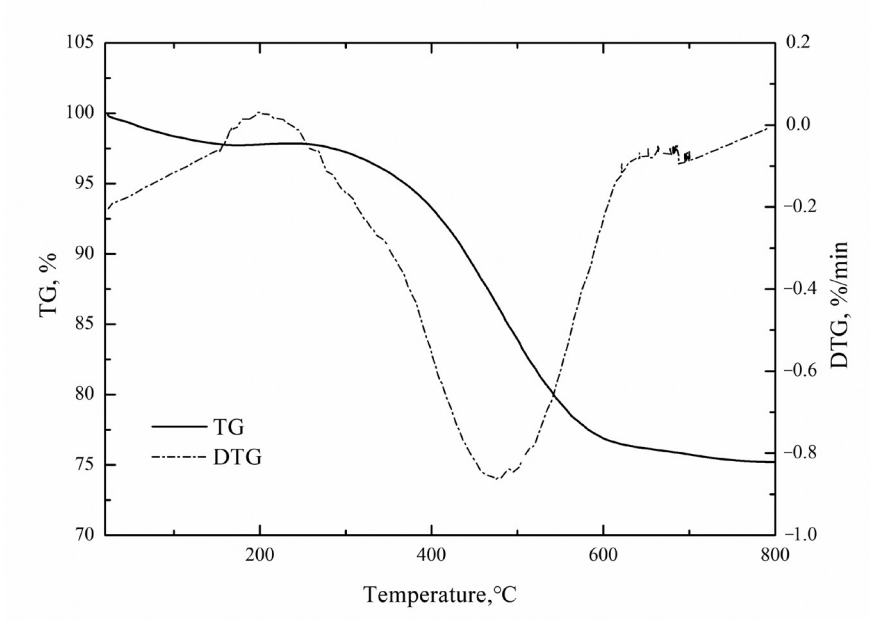

Fig. 1. TG and DTG curves of oil shale pyrolysis in Xinjiang.

Figure 1 shows the thermogravimetric (TG) and derivative thermogravimetric (DTG) curves of weight loss during the pyrolysis of Xinjiang oil shale. It can be clearly seen from Figure 1 that the main pyrolysis temperature range of oil shale is 350–600 °C. Based on the thermogravimetric data, the Coats–Redfern (CR) method [17–21] was used for kinetic analysis, and the pyrolysis reaction rate equation of oil shale was obtained as follows:

$$\alpha = 1 - e^{-Kt} = 1 - e^{-196868843.3 \times e^{-\frac{16891}{T} \times t}}, \tag{10}$$

where K is the rate constant, t is the pyrolysis time and T is the absolute temperature.

3.2. Simulation results and verification of oil shale porosity during pyrolysis

The average density of oil shale in Xinjiang is 2.35 g/cm^3, the average content of kerogen is 16.4%, and the average density of carbon residue after pyrolysis is 1.95 g/cm^3. In addition, according to aluminum retort analysis, the average percentage of shale oil is 8.05% and that of gas loss is 2.6%. The pyrolysis temperature of oil shale starts at 300 °C. To eliminate the influence of water on porosity, the porosity of oil shale at 200 °C was taken as the basic value of porosity before pyrolysis in this study, and the porosity values during pyrolysis at 300, 400 and 500 °C were quantitatively calculated.

In summary, the specific values of the parameters in this study were as follows: n = 1.95 g/cm^3, p_o = 16.4%, ρ_c = 1.95 g/cm^3, ρ_s = 2.35 g/cm^3,

ρ_o = 1.104 g/cm^3, p_c = 16.4% – 8.05% – 2.6% = 5.75%. Based on Equation (1), the porosity values of Xinjiang oil shale pyrolyzed at 350, 400, 450, 500 and 600 °C for a certain time were calculated and compared with the mercury injection test values under the same conditions (Table 2). The overall error was small and within the acceptable range.

Table 2. Comparison between calculated and experimental values of oil shale porosity during pyrolysis

Temperature, °C	Pyrolysis time, min	Measured value of porosity, %	Calculated porosity value, %	Absolute error, %
350	15	7.21	8.57	1.36
	30	7.38	9.87	2.49
	45	10.48	11.10	0.62
	60	9.39	12.27	2.88
400	15	8.52	15.94	7.42
	30	15.15	21.94	6.79
	45	18.78	26.07	7.29
	60	19.90	28.92	9.02
450	15	–	31.83	–
	30	27.70	34.78	7.08
	45	27.22	35.14	7.92
	60	38.66	35.18	3.48
500	15	36.33	35.19	1.14
	30	37.24	35.19	2.05
	45	33.43	35.19	1.76
	60	34.34	35.19	0.85
600	15	36.12	35.19	0.93
	30	34.76	35.19	0.43
	45	35.68	35.19	0.49
	60	36.06	35.19	0.87

3.3. Simulation results and verification of the elastic modulus of oil shale during pyrolysis

The compressive strength of oil shale after complete pyrolysis under different temperature conditions (i.e., the compressive strength of the oil shale skeleton) is fitted, as shown in Figure 2.

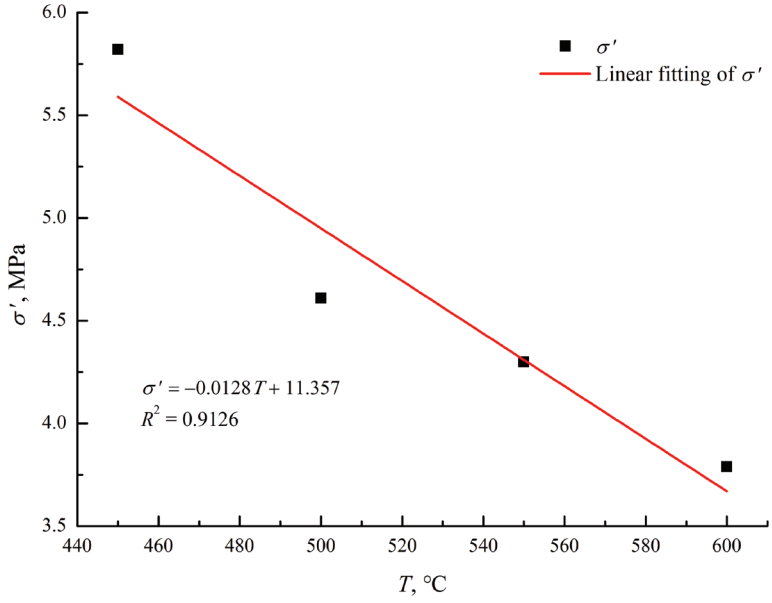

Fig. 2. Relationship between the skeletal strength and temperature of oil shale in Xinjiang.

The compressive strength of the oil shale skeleton has a linear decay trend with increasing temperature, and the relationship is as follows:

$$\sigma' = -0.0128\ T + 11.357. \tag{11}$$

The pyrolysis temperature of oil shale in Xinjiang started from 350 °C. To exclude the influence of moisture in oil shale on pore pressure, the compressive strength (σ_0 = 48.36 MPa) and elastic modulus (E_0 = 4229 MPa) of oil shale heated at 200 °C for 60 min were taken as the compressive strength and elastic modulus before pyrolysis.

The skeletal strength of oil shale before pyrolysis was calculated from Equation (11) as follows:

$$\sigma_0' = -0.0128 \times 200 + 11.357 = 8.80 \text{ MPa}. \tag{12}$$

The pore pressure provided by kerogen was as follows:

$$u = \sigma_0 - \sigma_0' = 48.36 - 8.80 = 39.56 \text{ MPa}. \tag{13}$$

The pore pressure provided by kerogen during pyrolysis was as follows:

$$u_t = u(1-a) = ue^{-Kt} = 39.56\ e^{-Kt}. \tag{14}$$

The elastic modulus of oil shale during pyrolysis was as follows:

$$E_t = \frac{E_0(\sigma' + u_t)}{\sigma_0} = \frac{4229(-0.0128\,T + 11.357 + 39.56\,e^{-Ae^{-\frac{D}{RT}}t})}{48.36}. \quad (15)$$

The elastic modulus of Xinjiang oil shale was calculated under the temperature conditions of 350, 400, 450, 500 and 600 °C for 60 min and compared with the measured values under the same conditions. The results are shown in Table 3, where it is visible that the calculated value of the elastic modulus of oil shale was very close to the test value, with a small error. This indicates that the assumptions and calculation methods proposed in this article are feasible.

Table 3. Comparison between calculated and experimental values of oil shale elastic modulus during pyrolysis

Temperature, °C	Measured value of elastic modulus, MPa	Calculated value of elastic modulus, MPa	Relative error, %
350	4072.80	3486.40	14.40
400	1463.50	1372.50	6.22
450	608.03	541.85	10.88
500	498.25	485.16	2.63
600	397.68	373.25	6.14

3.4. Calculation results of the oil shale permeability model during in-situ pyrolysis

According to Equation (9), the permeability of oil shale in Xinjiang during complete pyrolysis (400, 500 and 600 °C) under in-situ conditions (0.8 MPa) was simulated and calculated, and compared with the measured values. The results are shown in Table 4. As can be seen from the table, the calculated permeability of oil shale was close to the measured value, and the error was small. Compared with the initial permeability, the permeability of oil shale increased by three orders of magnitude after in-situ pyrolysis, changing from a water-impermeable layer before pyrolysis to a weakly permeable layer after pyrolysis, but it was still small overall.

Table 4. Permeability of oil shale in Xinjiang under in-situ pyrolysis conditions

Temperature, °C	Calculated value of permeability, mD	Measured value of permeability, mD
Room temperature	1.615E-3	2.217E-3
400	2.071	1.795
500	2.068	2.265
600	2.062	2.007

3.5. Physicochemical parameters and pollutants of oil shale leaching solution

The Xinjiang oil shale samples, which were completely pyrolyzed at room temperature and under different working conditions (400, 500 and 600 °C), were crushed and soaked according to a 1:10 solid–liquid ratio (mass ratio). The physicochemical parameters related to the leaching solution and the concentration of pollutants were determined by the multiparameter water quality monitoring instrument, atomic absorption spectrophotometer and liquid chromatograph (Tables 5, 6).

Table 5. Physicochemical parameters of Xinjiang oil shale leaching solution

Temperature, °C	Time, d	pH	Electrical conductivity, μS/cm
Room temperature	0	8.14	8
	5	8.46	776
	10	8.13	816
	15	8.22	852
400	0	8.14	8
	5	9.23	490
	10	9.22	591
	15	9.20	616
500	0	8.14	8
	5	9.61	493
	10	9.26	589
	15	9.18	625
600	0	8.14	8
	5	11.51	846
	10	11.66	1062
	15	11.68	1011

Table 6. Pollutants of Xinjiang oil shale leaching solution

Condition	Pb, μg/L	Cd, μg/L	T-Cr, mg/L	PAHs, μg/L
Room temperature + 15 d	Undetected	Undetected	Undetected	5.88
400 °C + 15 d	Undetected	Undetected	Undetected	6.96
500 °C + 15 d	0.66	Undetected	Undetected	7.09
600 °C + 15 d	1.84	Undetected	Undetected	7.83

The higher the pyrolysis temperature is, the easier it is for the material components of oil shale to enter underground water. In terms of the physicochemical properties of water, electrical conductivity increased with increasing pyrolysis temperature. In addition, the pyrolysis temperature affected the pH of groundwater around the oil shale, and the pH increased with increasing pyrolysis temperature. The pH data showed that the groundwater environment was alkaline, but at room temperature, 400 and 500 °C, the pH of groundwater was weakly alkaline; however, when the temperature reached 600 °C, the groundwater pH increased to 11.68, showing strong alkalinity. Furthermore, with the extension of soaking time, the conductivity and pH showed an increasing trend. After soaking for 10 days, the changes in conductivity and pH gradually became stable. Electrical conductivity represents the leaching level of pollutants from pyrolysis residues in groundwater. The change in electrical conductivity tended to be stable at the later stage of immersion, which meant that the concentration of pollutants in the solution also tended to be stable. The concentration of pollutants soaked for 15 days was sufficient to be considered close to the maximum value.

In terms of common heavy metals and organic pollutants in groundwater, such as lead (Pb), cadmium (Cd), total chromium (T-Cr), and polycyclic aromatic hydrocarbons (PAHs), the concentration of each pollutant was small and existed in groundwater in trace amounts. Among them, Cd and T-Cr were not detected, and Pb was not detected at the low-temperature stage; trace amounts were detected only when the pyrolysis temperature was higher than 500 °C. PAHs were detected at all conditions. The concentrations of Pb and PAHs in groundwater increased with increasing pyrolysis temperature, which meant that high pyrolysis temperature was more likely to damage the groundwater environment.

3.6. Groundwater pollutant migration in the in-situ pyrolysis mining area of oil shale

To build the hydrogeological conceptual model of the mining area, combined with the aforementioned physical and mechanical model of the in-situ pyrolysis of oil shale, and taking the results of the soaking experiment as the pollutant source concentration, the MODFLOW software was used to simulate the diffusion and migration of pollutants in groundwater under different in-situ pyrolysis conditions of oil shale (400, 500 and 600 °C).

(1) Establishment of the hydrogeological model

According to the geological data of the oil shale sample collection area in Xinjiang, the following hydrogeological conceptual model was constructed:

1) The stratum in the study area is divided into three layers from top to bottom: the first layer is the surface quaternary loose sediment layer (Q_4, aeration zone layer, 40 m thick), the second is the oil shale layer of the Lucaogou Formation of the Upper Jijicaozi Group of the Permian System

(P_2l, water resistant layer, 30 m thick), and the third is the underlying fine sandstone layer (confined aquifer, 10 m thick), with a total thickness of 80 m.

2) The study area covered 5 × 5 km. The groundwater in the area is confined water, and the confined aquifer is a fine sandstone layer. The eastern and western boundaries of this aquifer are connected to the bedrock, forming an aquiclude. The northern and southern boundaries of the aquifer are both fixed head boundaries, with the artesian heights of 115 m in the northern boundary and 124 m in the southern boundary.

3) There is an oil shale in-situ pyrolysis mining area (900 × 700 m) located in the southeastern part of the research area.

4) There is no surface water system in the study area, with an average annual precipitation and a historical maximum annual precipitation of approximately 180 and 330 mm, respectively.

5) Based on experimental and previous research data, the hydrogeological parameters of each layer in the area are as follows:

Quaternary loose sediment layer (Q_4): the permeability coefficient $k_x = k_y$ = 1.8E-5, m/s; k_z = 1.8E-6, m/s; water storage coefficient S_s = 1E-9, L/m; specific yield S_y = 0.2; effective porosity is 0.15, and total porosity is 0.30.

Lucaogou oil shale layer (P_2l): without pyrolysis, the water storage coefficient S_s = 1E-1, L/m; and the specific yield S_y = 1E-9. Under the condition of 400–600 °C: the water storage coefficient S_s = 1E-9, L/m; and the specific yield S_y = 1E-8. The permeability parameters vary with temperature and pressure conditions, and were calculated based on Equation (9).

Fine sandstone formation: the permeability coefficient $k_x = k_y$ = 1.04E-5, m/s; k_z = 1.04E-6, m/s; water storage coefficient S_s = 1E-5, L/m; specific yield S_y = 0.21; effective porosity is 0.33, and total porosity is 0.33.

The values of longitudinal and transverse dispersion in the study area were 10 m and 1 m, respectively.

6) The study area was divided into a grid of 50 × 50 m, and the movement of groundwater pollutants was simulated at pyrolysis temperatures of 400, 500 and 600 °C in the most unfavorable situation (precipitation was the historical annual maximum value of 330 mm, the effective porosity of oil shale was equal to total porosity, the source concentration of pollutants in oil shale was determined by the maximum value under each working condition, and there was no adsorption or chemical reaction in the whole process). The simulation period was 20 years (7300 days).

(2) The simulation results are as follows:

1) Transport of pollutants in the in-situ pyrolysis mining area at 400 °C

As seen in Figure 3, under the pyrolysis temperature of 400 °C, only PAHs were found in groundwater. Twenty years after the completion of mining, from the perspective of the spatial distribution of concentration, PAHs were mainly concentrated in the pyrolysis mining section of the second layer of oil shale, with a maximum concentration of 0.007 mg/L. The concentration of PAHs

(a)

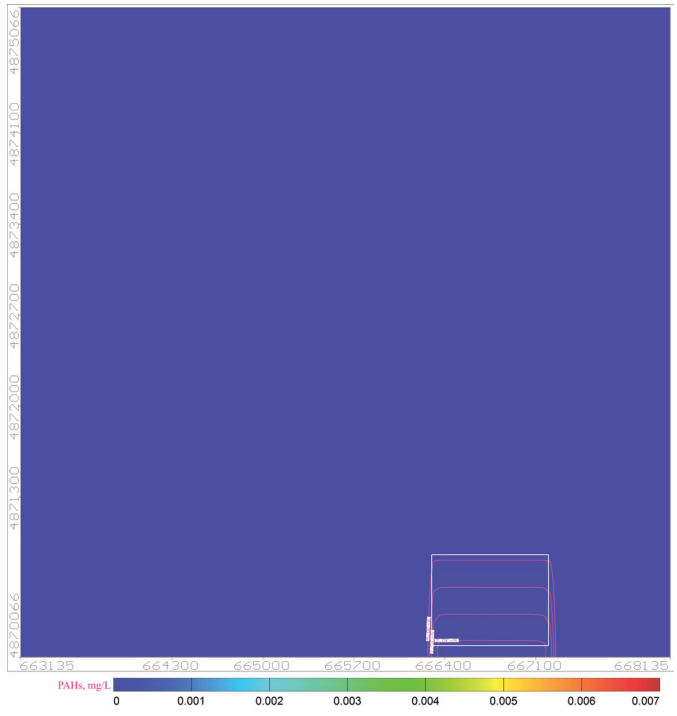
4875066
4874100
4873400
4872700
4872000
4871300
4870066
663135
664300
665000
665700
666400
667100
668135
PAHs, mg/L
0
0.001
0.002
0.003
0.004
0.005
0.006
0.007

(b)

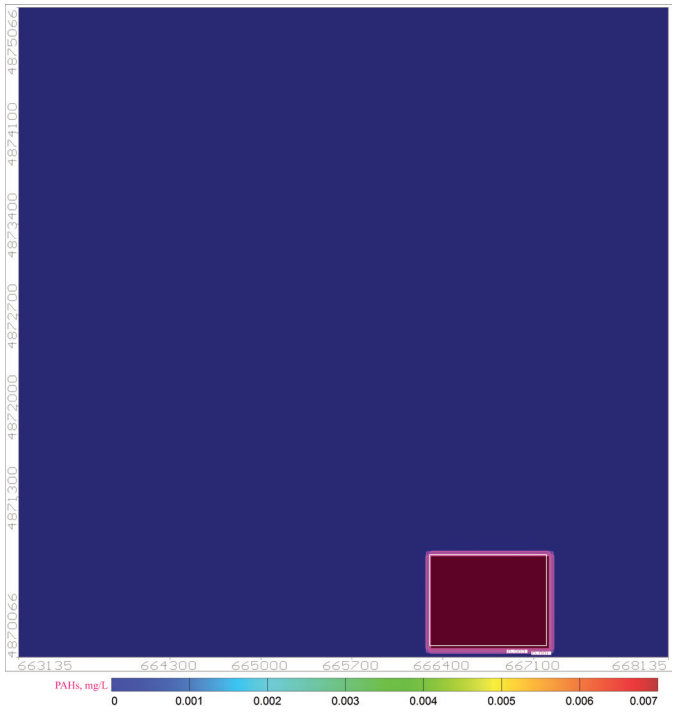
4875066
4874100
4873400
4872700
4872000
4871300
4870066
663135
664300
665000
665700
666400
667100
668135
PAHs, mg/L
0
0.001
0.002
0.003
0.004
0.005
0.006
0.007

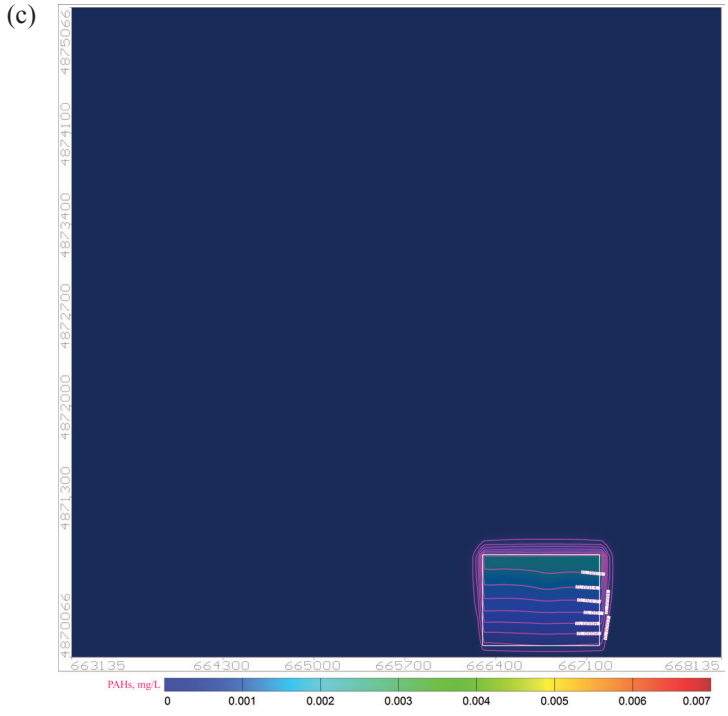

Fig. 3. Distribution of pollutant transport at a pyrolysis temperature of 400 °C: (a) in the first layer after 20 years, (b) in the second layer after 20 years, (c) in the third layer after 20 years.

in the first layer was the smallest, with a maximum of only 2.5E-5 mg/L. The concentration of PAHs in the third layer was relatively high, and the PAHs were mainly distributed in the contact area with pyrolytic oil shale, with a maximum concentration of 0.0018 mg/L.

2) Transport of pollutants in the in-situ pyrolysis mining area at 500 °C

As seen in Figure 4, under the pyrolysis temperature of 500 °C, groundwater contained both Pb and PAHs. The spatial distribution of the two pollutants was extremely uneven, but they were mainly concentrated in the second layer of the oil shale pyrolysis mining section and its surrounding areas. The maximum concentrations of Pb and PAHs in the second layer were 7E-4 mg/L and 8E-3 mg/L, respectively. The contents of Pb and PAHs in the first layer were the lowest, and the maximum concentrations were only 2.5E-6 mg/L and 2.5E-5 mg/L, respectively. The pollutant content in the third layer was between that of the first and second layers, and the maximum concentrations of Pb and PAHs were 1.8E-4 mg/L and 1.8E-3 mg/L, respectively.

(a)

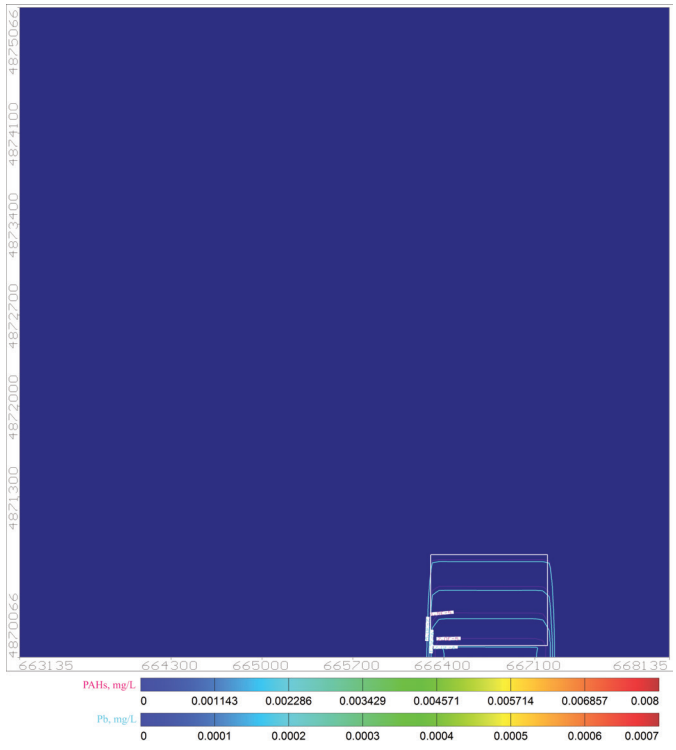
4875066
4874100
4873400
4872700
4872000
4871300
4870066
663135
664300
665000
665700
666400
667100
668135
PAHs, mg/L
0
0.001143
0.002286
0.003429
0.004571
0.005714
0.006857
0.008
Pb, mg/L
0
0.0001
0.0002
0.0003
0.0004
0.0005
0.0006
0.0007

(b)

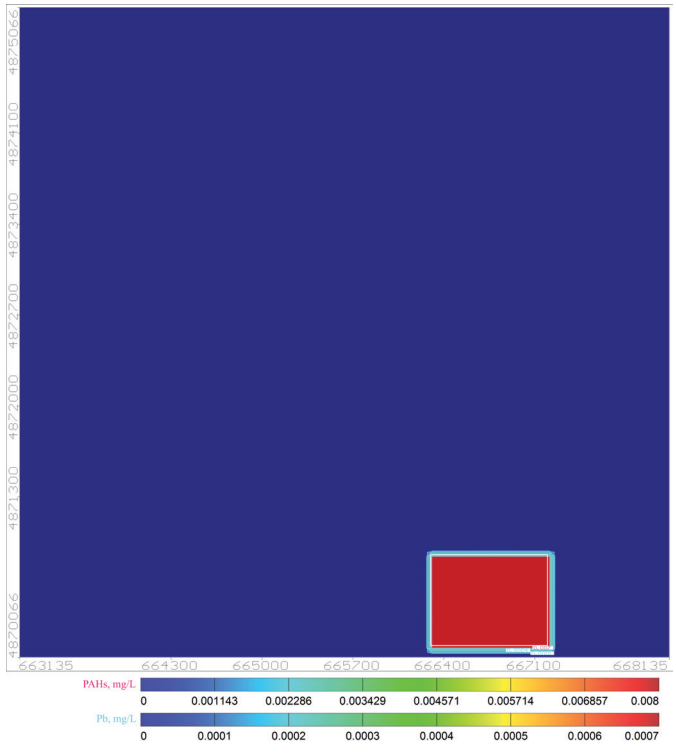
4875066
4874100
4873400
4872700
4872000
4871300
4870066
663135
664300
665000
665700
666400
667100
668135
PAHs, mg/L
0
0.001143
0.002286
0.003429
0.004571
0.005714
0.006857
0.008
Pb, mg/L
0
0.0001
0.0002
0.0003
0.0004
0.0005
0.0006
0.0007

(c)

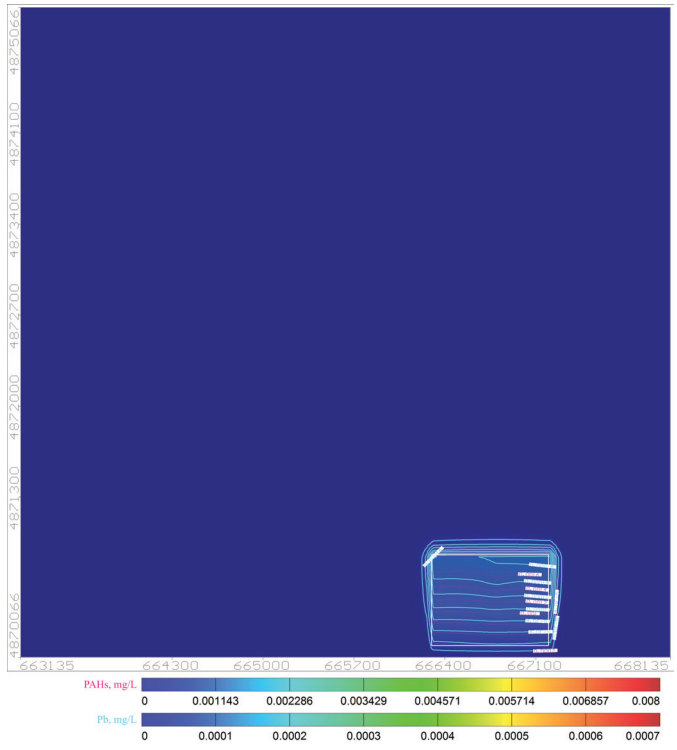

Fig. 4. Distribution of pollutant transport at a pyrolysis temperature of 500 °C: (a) in the first layer after 20 years, (b) in the second layer after 20 years, (c) in the third layer after 20 years.

3) Transport of pollutants in the in-situ pyrolysis mining area at 600 °C

As seen in Fiure 5, similar to the situation at 500 °C, the Pb and PAHs under the pyrolysis temperature of 600 °C were also mainly concentrated in and around the oil shale pyrolysis mining section. The maximum concentrations of Pb and PAHs in the second layer were 2E-3 mg/L and 8E-3 mg/L, respectively. The contents of Pb and PAHs in the first layer were the lowest, and the maximum concentrations were only 6E-6 mg/L and 2.5E-5 mg/L, respectively. The maximum concentrations of Pb and PAHs in the third layer were 5E-4 mg/L and 2E-3 mg/L, respectively.

(a)

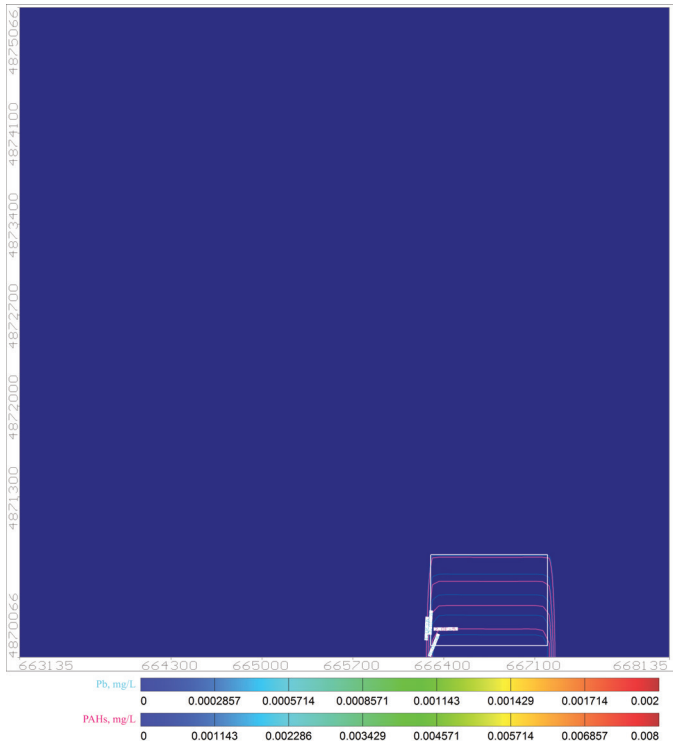
4825066
4824100
4823400
4822700
4822000
4821300
4820066
663135
664300
665000
665700
666400
667100
668135
Pb, mg/L
0 0.0002857 0.0005714 0.0008571 0.001143 0.001429 0.001714 0.002
PAHs, mg/L
0 0.001143 0.002286 0.003429 0.004571 0.005714 0.006857 0.008

(b)

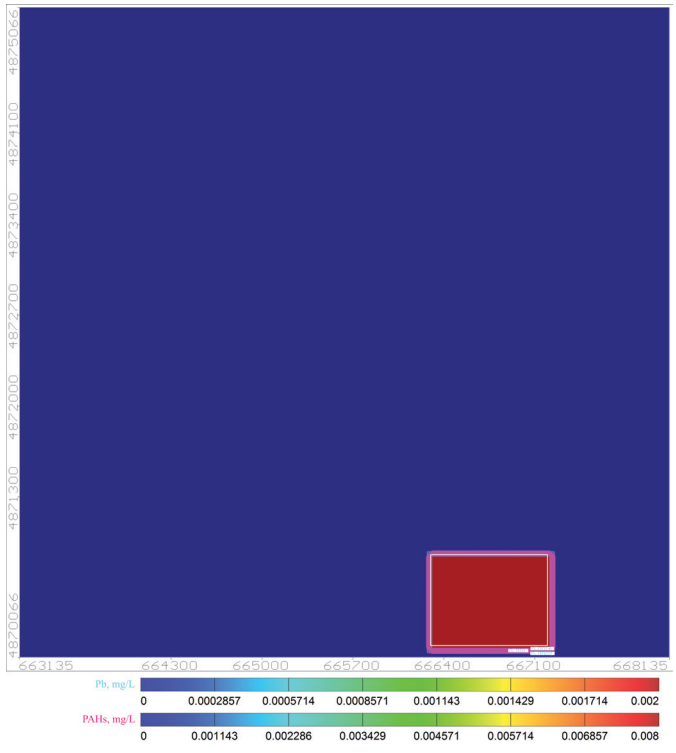
4825066
4824100
4823400
4822700
4822000
4821300
4820066
663135
664300
665000
665700
666400
667100
668135
Pb, mg/L
0 0.0002857 0.0005714 0.0008571 0.001143 0.001429 0.001714 0.002
PAHs, mg/L
0 0.001143 0.002286 0.003429 0.004571 0.005714 0.006857 0.008

(c)

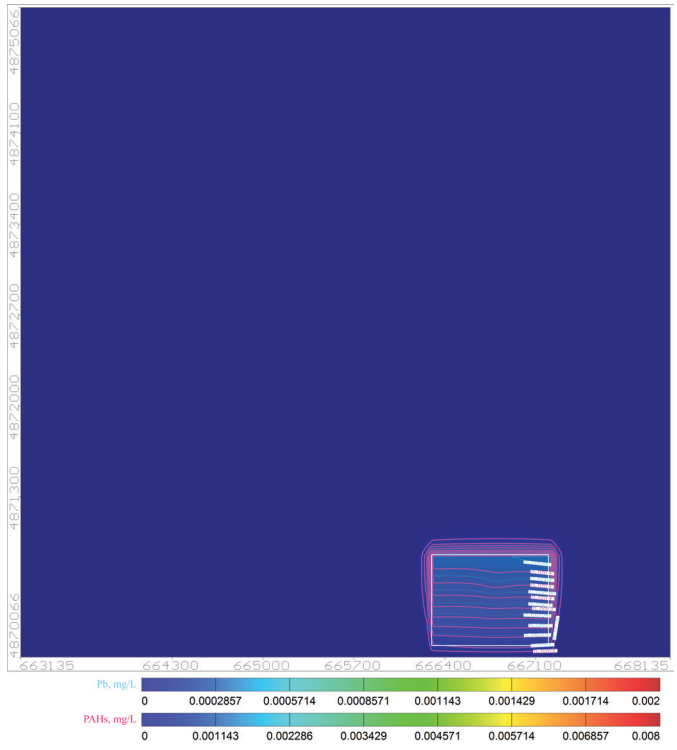

Fig. 5. Distribution of pollutant transport at a pyrolysis temperature of 600 °C: (a) in the first layer after 20 years, (b) in the second layer after 20 years, (c) in the third layer after 20 years.

The above simulation results reveal that 20 years after the completion of the in-situ pyrolysis of oil shale, even under the most adverse circumstances, since the permeability of oil shale after pyrolysis remained very low, the pollutants were still mainly concentrated in the pyrolyzed oil shale layer. The movement and migration amounts in the upper phreatic layer and the bottom fine sandstone layer were very small, the pollutant concentration was low, and the groundwater quality was basically not affected.

4. Conclusions

1. Based on the mechanism of changes in the physical and mechanical properties of oil shale during pyrolysis, combined with the pyrolysis reaction kinetics, the porosity model and elastic modulus model of oil shale during pyrolysis were established. On the basis of these models, combined with the theory of rock mechanics and the Kozeny–Carman equation, the

permeability model of oil shale during in-situ pyrolysis was derived. The calculated results were in good agreement with the experimental results, and the error was small.
2. Both the electrical conductivity and pH of the immersion solution increased with the pyrolysis temperature, especially at 600 °C, and pH increased to 11.68, which is strongly alkaline. The concentrations of pollutants were small and existed in trace amounts. The concentrations of Pb and PAHs increased with the pyrolysis temperature. This means that high-temperature pyrolysis is more likely to cause damage to the groundwater environment.
3. The numerical simulation results showed that under different pyrolysis temperatures, due to the low permeability of oil shale after pyrolysis, the pollutants were mainly concentrated in the pyrolyzed oil shale layer, and their movement and migration amounts in the upper phreatic layer and the bottom fine sandstone layer were very small. The concentration of pollutants was low, and the groundwater quality was basically not affected.
4. Although the high temperature pyrolysis rate is fast, the energy cost is high, and the underground water environment is more likely to be destroyed, making the underground water body become strongly alkaline. From the perspective of economy and environmental protection, it is suggested that the pyrolysis temperature of oil shale should not be too high, and 400–500 °C is appropriate.

Acknowledgments

This work was supported by the National Natural Science Foundation of China (grant No. 51604182), Hebei Key Research Projects, China (grant No. 21374104D), Hebei Natural Science Foundation, China (grants No. E2020402075, D2022402005), and the Science and Technology Project of Hebei Education Department, China (grant No. ZD2021309). The publication costs of this article were partially covered by the Estonian Academy of Sciences.

REFERENCES

1. Kang, Z., Yang, D., Zhao, Y., Hu, Y. Thermal cracking and corresponding permeability of Fushun oil shale. *Oil Shale*, 2011, **28**(2), 273–283. https://doi.org/10.3176/oil.2011.2.02
2. Eseme, E., Krooss, B. M., Littke, R. Evolution of petrophysical properties of oil shales during high-temperature compaction tests: Implications for petroleum expulsion. *Mar. Petrol. Geol*., 2012, **31**(1), 110–124. https://doi.org/10.1016/j.marpetgeo.2011.11.005
3. Bai, F., Sun, Y., Liu, Y., Guo, M. Evaluation of the porous structure of Huadian

oil shale during pyrolysis using multiple approaches. *Fuel*, 2017, **187**(1), 1–8. https://doi.org/10.1016/j.fuel.2016.09.012

4. Tang, H., Zhao, Y., Kang, Z., Lv, Z., Yang, D., Wang, K. Investigation on the fracture-pore evolution and percolation characteristics of oil shale under different temperatures. *Energies*, 2022, **15**(10), 1–14. https://doi.org/10.3390/en15103572
5. Zhao, J., Yang, L., Yang, D., Kang, Z., Wang, L. Study on pore and fracture evolution characteristics of oil shale pyrolysed by high-temperature water vapour. *Oil Shale*, 2022, **39**(1), 79–95. https://doi.org/10.3176/oil.2022.1.05
6. Geng, Y., Liang, W., Liu, J., Cao, M., Kang, Z. Evolution of pore and fracture structure of oil shale under high temperature and high pressure. *Energy Fuels*, 2017, **31**(10), 10404–10413. https://doi.org/10.1021/acs.energyfuels.7b01071
7. Geng, Y., Liang, W., Liu, J., Kang, Z., Wu, P., Jiang, Y. Experimental study on the variation of pore and fracture structure of oil shale under different temperatures and pressures. *Chin. J. Rock Mech. Eng.*, 2018, **37**(11), 2510–2519 (in Chinese with English abstract). https://doi.org/10.13722/j.cnki.jrme.2018.0623
8. Geng, Y., Liang, W., Liu, J., Wu, P., Zhao, J. Experimental study on the law with permeability of Fushun oil shale under high temperature and triaxial stresses. *J. Taiyuan Univ. Tech.*, 2019, **50**(3), 272–278 (in Chinese with English abstract). https://doi.org/10.16355/j.cnki.issn1007-9432tyut.2019.03.002
9. Yang, D., Wang, G., Kang, Z., Zhao, J., Lv, Y. Experimental investigation of anisotropic thermal deformation of oil shale under high temperature and triaxial stress based on mineral and micro-fracture characteristics. *Nat. Res. Res.*, 2020, **29**(1), 3987–4002. https://doi.org/10.1007/s11053-020-09663-x
10. He, W., Meng, Q., Lin, T., Wang, R., Liu, X., Ma, S., Li, X., Yang, F., Sun, G. Evolution of in-situ permeability of low-maturity shale with the increasing temperature, Cretaceous Nenjiang Formation, northern Songliao Basin, NE China. *Petrol. Explor. Dev.*, 2022, **49**(3), 453–464 (in Chinese with English abstract). https://doi.org/10.11698/PED.20210881
11. Zhao, L., Cheng, Y., Zhang, Y. Pore and fracture scale characterization of oil shale at different microwave temperatures. *Oil Shale*, 2023, **40**(2), 91–114. https://doi.org/10.3176/oil.2023.2.01
12. Brandt, A. R. Converting oil shale to liquid fuels: Energy inputs and greenhouse gas emissions of the shell in situ conversion process. *Environ. Sci. Technol.*, 2008, **42**(19), 7489–7495. https://doi.org/10.1021/es800531f
13. Zhang, F., Liu, Z., Li, C., Tao, Y., Lü, C. Risk assessment of the atmospheric environment during in-situ oil shale exploitation. *Sci. Tech. Rev.*, 2013, **31**(26), 44–47 (in Chinese with English abstract). https://doi.org/10.3981/j.issn.1000-7857.2013.26.006
14. Hu, S., Wu, H., Liang, X., Xiao, C., Zhao, Q., Cao, Y., Han, X. A preliminary study on the eco-environmental geological issue of in-situ oil shale mining by a physical model. *Chemosphere*, 2022, **287**(1), 131987. https://doi.org/10.1016/j.chemosphere.2021.131987
15. Cai, M. *Rock Mechanics and Engineering*. Science Press, Beijing, 2002 (in Chinese).

16. Porter, L. B., Ritzi, R. W., Mastera, L. J. The Kozeny-Carman equation with a percolation threshold. *Groundwater*, 2013, **51**(1), 92–99. https://doi.org/10.1111/j.1745-6584.2012.00930.x
17. Liu, J., Liang, W., Kang, Z., Lian, H., Geng, Y. Study on the quantitative model of oil shale porosity in the pyrolysis process based on pyrolysis kinetics. *Oil Shale*, 2018, **35**(2), 128–143. https://doi.org/10.3176/oil.2018.2.03
18. Coats, A. W., Redfern, J. P. Kinetic parameters from thermogravimetric data. *Nature*, 1964, **201**, 68–69. https://doi.org/10.1038/201068A0
19. Braun, R. L., Rothman, A. J. Oil-shale pyrolysis: Kinetics and mechanism of oil production. *Fuel*, 1975, **54**(2), 129–131. https://doi.org/10.1016/0016-2361(75)90069-1
20. Liu, J., Liang, W., Lian, H., Li, L. Study on the quantitative model of the elastic modulus of oil shale during pyrolysis. *Oil Shale*, 2018, **35**(4), 327–338. https://doi.org/10.3176/oil.2018.4.03
21. Li, L., Liu, J., Geng, Y. Study on the permeability of oil shale during in situ pyrolysis. *Oil Shale*, 2021, **38**(2), 119–136. https://doi.org/10.3176/oil.2021.2.02